

# Effects of anchoring group number and conjugated structure of Fe-bipyridyl/phenanthroline complexes on the photocatalytic activity of TiO<sub>2</sub> under visible light

Dan Wang<sup>a</sup>, Qingkun Shang<sup>a,b,\*</sup>, Xinyue Wang<sup>a</sup>, Hongyu Guan<sup>a</sup>, Qin Lu<sup>b,c</sup>, Shik Chi Tsang<sup>b,\*\*</sup>

<sup>a</sup>Faculty of Chemistry, Northeast Normal University, Changchun 130024, China

<sup>b</sup>Department of Chemistry, University of Oxford, Oxford OX1 3QR, UK

<sup>c</sup>Naval Research Laboratory, Chemistry Division, Washington D.C. 20375-5342, USA

**Abstract** Complex [Fe<sup>II</sup>(dcbpy)<sub>3</sub>] (dcbpy=2,2'-bipyridine-4,4'-dicarboxylic acid) had been synthesized through a simple method and acted as a photosensitizer to improve the photocatalytic activity of TiO<sub>2</sub> under visible light irradiation. X-ray Diffraction (XRD), X-ray Photoelectron Spectroscopy (XPS), UV-Vis spectroscopy, Raman spectra, Scanning Electron Microscope (SEM) and Transmission Electron Microscope (TEM) had been used to characterize the structure and morphology of [Fe<sup>II</sup>(dcbpy)<sub>3</sub>]/TiO<sub>2</sub>. It exhibited enhanced photocatalytic activity on photodecomposition of phenol in aqueous solution under visible light irradiation comparing to that of pure TiO<sub>2</sub>. In order to reveal the effects of anchoring group number and conjugated structure of Fe-complex on the photocatalytic activity of TiO<sub>2</sub> under visible light four other complexes [Fe<sup>II</sup>(dcbpy)(bpy)<sub>2</sub>], [Fe<sup>II</sup>(dcbpy)<sub>2</sub>(bpy)], [Fe<sup>II</sup>(dcbpy)(phen)<sub>2</sub>], and [Fe<sup>II</sup>(dcbpy)<sub>2</sub>(phen)] (bpy=2,2'-bipyridine, phen=1,10-Phenanthroline) were used to compose a series of photocatalysts with TiO<sub>2</sub> and applied to the degradation of phenol under the same visible light condition.

Encouragingly, all these four composite photocatalysts as same as  $[\text{Fe}^{\text{II}}(\text{dcbpy})_3]/\text{TiO}_2$  show significantly enhanced photocatalytic activity in contrast to  $\text{TiO}_2$ . Their different performances on the degradation of phenol derived from their different interfacial interaction and electron transfer between complexes and  $\text{TiO}_2$  surface were discussed in detail. Based on a series of research works of dynamical process of photocatalytic degradation of phenol, recycling stability, absorption spectra, photoelectrochemistry performance and cyclic voltammetry the possible electron transfer pathway and mechanism had been proposed, which can reasonably explain the different photocatalytic activities of these five novel catalysts.

**Keyword:** anchoring group number; conjugated structure; interfacial interaction; electron transfer pathway; visible light photocatalytic activity of  $\text{TiO}_2$

## **Introduction**

$\text{TiO}_2$  has been one of the most popular photocatalysts because of its low cost, low toxicity, high physical and chemical stability. However, its wide band gap (3.2 and 3.0 eV for anatase and rutile phase, respectively) results its inactivity in the visible light region, thus limits its practical applications greatly. The visible light active  $\text{TiO}_2$  photocatalyst currently under development can be divided into two categories: (1) doped  $\text{TiO}_2$  by impurities such as metal/nonmetal ions <sup>[1-3]</sup> or sensitized by dyes <sup>[4-7]</sup> and (2) constructed new composite materials with narrow band gap semiconductor <sup>[8, 9]</sup>. Dye sensitization of  $\text{TiO}_2$  has been extensively studied as a mean of visible light activation <sup>[10-15]</sup>.

One generally accepted mechanism of sensitizing  $\text{TiO}_2$  under visible light is indirect charge

transfer between sensitizer and TiO<sub>2</sub>. Dye molecules attached on the surface of TiO<sub>2</sub> via weak van der Waals interaction. Electrons transfer from excited dye to the conduction band of TiO<sub>2</sub> under visible light irradiation. Subsequently, molecules of oxygen on the surface of TiO<sub>2</sub> scavenge the electrons to promote the generation of superoxide radicals and hydrogen peroxide radicals. These radicals attack the aromatic rings of organic pollutants forming intermediates and mineralizing them to carbon dioxide and water. Ru-bipyridyl complexes have been used as sensitizers in photocatalytic degradation of organic compounds, hydrogen production and dye-sensitized solar cells (DSSCs), following this mechanism. For example, Cho, and Bae et al. reported that TiO<sub>2</sub> particles sensitized by ruthenium bipyridyl complexes degraded carbon tetrachloride and trichloroacetate in a reductive path [16-18].

Another mechanism of sensitizing TiO<sub>2</sub> under visible light is the direct charge transfer between surface adsorbate and TiO<sub>2</sub>. The electrons are photo excited directly from the ground state of the adsorbate to the conduction band of TiO<sub>2</sub> by forming the charge transfer complex on the surface of TiO<sub>2</sub>. According to the report from Wang et al. [19] the formation of a complex between catechol and TiO<sub>2</sub> created a broad new absorption band centered at 390nm and extended into the visible region at 600 nm. Thus the excitation of visible light induced the direct transfer of electron from the organic substrate into the conduction band of TiO<sub>2</sub>.

In the research of TiO<sub>2</sub> sensitized by dye one important question has attracted more attention. What is the impact of the interfacial interaction between dye and TiO<sub>2</sub> surface on the electron transfer pathway and sensitization mechanism? Bae and Choi investigated the effects of anchoring group carboxylate and phosphonate in Ru-bipyridyl complexes sensitized TiO<sub>2</sub> on hydrogen production under visible light and their photoelectrochemical performance in DSSCs [13]. They

found that the type and the number of anchoring groups modified the intrinsic properties of the surface chemical bonds, as well as the visible light absorbing capability and the surface charge of TiO<sub>2</sub>.

Despite the remarkable improvements in TiO<sub>2</sub> properties sensitizing by ruthenium bipyridyl complexes, several challenges have to be overcome for real environmental applications, such as reducing the toxicity of the photocatalysts and the usage of expensive noble metals. In this paper, [Fe<sup>II</sup>(dcbpy)<sub>3</sub>] (dcbpy=2,2'-bipyridine-4,4'-dicarboxylic acid), a complex easy to synthesize, low in toxicity and cost, was used to sensitize TiO<sub>2</sub> photocatalyst. The enhanced photocatalytic activity of TiO<sub>2</sub> on the degradation of phenol under visible light was observed. Furthermore, in order to investigate the effects on the photocatalytic activity of TiO<sub>2</sub> arising from the anchoring group number and the conjugated structure of organic ligands, four other Fe complexes, [Fe<sup>II</sup>(dcbpy)(bpy)<sub>2</sub>], [Fe<sup>II</sup>(dcbpy)<sub>2</sub>(bpy)], [Fe<sup>II</sup>(dcbpy)(phen)<sub>2</sub>], and [Fe<sup>II</sup>(dcbpy)<sub>2</sub>(phen)] (bpy=2,2'-bipyridine, phen=1,10-Phenanthroline) were used to construct a series of photocatalysts with TiO<sub>2</sub> and applied to the degradation of phenol under the same visible light condition. Like [Fe<sup>II</sup>(dcbpy)<sub>3</sub>]/TiO<sub>2</sub>, these four composite photocatalysts show significantly enhanced photocatalytic activity in contrast to TiO<sub>2</sub>. Their different performances on the degradation of phenol derived from their different interfacial interaction and electron transfer between complexes and TiO<sub>2</sub> surface were discussed in detail, including not only the anchoring group number and conjugated structure of Fe-complexes but also the phase structure, crystal parameter and visible light absorbing capability of TiO<sub>2</sub>. The possible electron transfer pathway and mechanism proposed in this paper will provide important insight into the design of novel and effective TiO<sub>2</sub> photocatalysts with visible light harvesting.

## 2. Experimental

### 2.1 Materials

All chemicals were of analytical grade and used as received, without further purification. All solutions were prepared using deionized water (resistivity 18.2 M $\Omega$ ·cm) obtained from a Millipore synergy water purification system (USA).

### 2.2 Synthesis

**Synthesis of TiO<sub>2</sub>.** TiO<sub>2</sub> nano-particles were prepared via hydrothermal method by adopting the same synthesis procedure as reported in our previous work [20]. Briefly, tetrabutyltitanate (2.0 mL) was added dropwise to absolute ethyl alcohol (5.0mL) under magnetic stirring. A yellow transparent solution was formed. To this solution, deionized water (3.0mL) was slowly added in 0.5h under continuous stirring. The mixture was then transferred to a 25 mL autoclave equipped with poly-tetrafluoroethylene (PTFE). The sample was heated at 120°C for 2h and then cooled to room temperature naturally. The white precipitate was collected by centrifugal separation, and washed with deionized water and absolute ethyl alcohol four times in turn before it was dried in vacuum oven at 80°C for 12h. This precursor was then calcined at 500°C for 4h to form TiO<sub>2</sub> nanoparticle.

**Synthesis of iron complexes** [Fe<sup>II</sup>(dcbpy)<sub>3</sub>] was synthesized as described below. 2,2'-bipyridine -4,4'-dicarboxylic acid (H<sub>2</sub>dcbpy) (0.073g) was dissolved in DMSO (60mL) at 25°C (colorless transparent solution A). FeSO<sub>4</sub>·7H<sub>2</sub>O (0.0278g) was dissolved in deionized water

(15mL) at 25°C (pale green close to colorless transparent solution B). Solution B was then added slowly to solution A under magnetic stirring and the color of resulting mixture turned to deep pink immediately. The mixture was continuously stirred for 2h and the deep pink precipitate,  $[\text{Fe}^{\text{II}}(\text{dcbpy})_3]$ , was obtained by centrifugal separation and dried at 80°C for 12h.

Other four Fe complexes,  $[\text{Fe}^{\text{II}}(\text{dcbpy})(\text{bpy})_2]$ ,  $[\text{Fe}^{\text{II}}(\text{dcbpy})_2(\text{bpy})]$ ,  $[\text{Fe}^{\text{II}}(\text{dcbpy})(\text{phen})_2]$ , and  $[\text{Fe}^{\text{II}}(\text{dcbpy})_2(\text{phen})]$ , were synthesized under the same condition but with different ratios of organic ligands. It was shown in Table 1. The images of five Fe complex aqueous solutions and their structures were displayed in Fig. 1.

*(Embed Table 1. Amount of organic ligands to prepare Fe complex)*

*(Embed Figure 1. The images of five Fe complex aqueous solutions and their structures)*

**Preparation of Fe complex/TiO<sub>2</sub> photocatalysts.** An aqueous mixture of Fe complex (2% mass ratio to TiO<sub>2</sub>) and TiO<sub>2</sub> was first prepared by adding TiO<sub>2</sub> powder to a Fe complex solution under 1h continuous stirring. The mixture was then transferred to a 10mL PTFE equipped autoclave. The autoclave was sealed, and kept at selected temperatures for 3-12h. After the reaction the autoclave was cooled to room temperature and the photocatalyst was collected using centrifugation followed by washing with deionized water and drying at 80 °C.

### 2.3 Characterization of the photocatalysts

The crystal structures of the prepared photocatalysts were examined by X-ray diffraction (XRD) using a Kigaku.D/Max-rA with Cu K radiation. A high resolution full band micro Raman

spectrometer HR800 was used to collect the Raman spectra (equipped with a 488nm laser). UV/VIS absorption spectra and UV-visible diffuse reflectance spectra (DRS) were obtained in the range between 200 and 800 nm using a UV-Vis-NIR spectrophotometer (CARY500Scan). The morphologies and sizes of the photocatalysts were characterized on a scanning electron microscopic (SEM, XL30ESEM-FEG), and a transmission electron microscopic (TEM, JEOL 100 CX II) combined with an energy-dispersive X-ray spectroscopy (EDS) for determining the chemical composition. X-ray photoelectron spectroscopy (XPS) data were obtained using a Thermo Scientific ESCALAB 250Xi photoelectron spectrometer. Ground-state redox potentials of Fe complexes were determined with a standard three-electrode configuration CHI830b using a modified glassy carbon (GC) electrode serving as the working electrode, and a platinum wire and Ag/AgCl (in saturated KCl solution) serving as the counter and reference electrodes, respectively.

#### **2.4 Photodegradation experiments**

The photocatalytic experiments were performed by the following procedure. Fifty mg photocatalyst was dispersed in 50 mL phenol ( $10 \text{ mg}\cdot\text{L}^{-1}$ ) solution in a quartz glass reactor, and stirred in the dark for 30 min to establish the adsorption-desorption equilibrium. The suspension was irradiated from the top of the reactor by a Xe lamp (300W) with a cut-off filter ( $\lambda > 400 \text{ nm}$ ). The condensate water was used to dissipate the heat generated from the illumination to maintain a reaction temperature at  $25 \pm 2 \text{ }^\circ\text{C}$ . At a certain time interval, 5 mL reaction mixture was withdrawn, and centrifuged to collect the supernatant which was then analyzed via a colorimetric method using ammonia buffer solution, 4-amino-Antipyrine and potassium ferricyanide. The color change was monitored at 510 nm using a UV-Vis spectrophotometer.

### 3. Results and discussion

#### 3.1 Structural properties of $[Fe^{II}(dcbpy)_3]/TiO_2$

The phase structures and crystal parameters of  $[Fe^{II}(dcbpy)_3]/TiO_2$  prepared at different hydrothermal temperatures were measured using XRD analysis and shown in Fig. 2a. Comparing to standard pattern of anatase (JCPDS 21-1272), pure  $TiO_2$  and three  $[Fe^{II}(dcbpy)_3]/TiO_2$  photocatalysts prepared under different temperatures all had a single phase anatase. There were no obvious diffraction peaks derived from the  $[Fe^{II}(dcbpy)_3]$  complex, suggesting that the phase structures of  $TiO_2$  did not change in the photocatalysts. The crystallite sizes of these photocatalysts were calculated using Debye Scherrer equation and given in Table 2. The crystallite sizes of three photocatalysts (23.81, 23.85, 23.92nm) are larger than that of  $TiO_2$  (23.76 nm). The crystal lattice parameters a, b, and c of  $[Fe^{II}(dcbpy)_3]/TiO_2$  prepared at 100°C are very similar to those of  $TiO_2$ , but the lattice parameters of two other photocatalysts, prepared at 80 °C and 120 °C, differ from those of pure  $TiO_2$ .

*(Embed Figure 2(a) XRD patterns for  $[Fe^{II}(dcbpy)_3]/TiO_2$  prepared at different temperatures. (b) Raman spectra of  $[Fe^{II}(dcbpy)_3]/TiO_2$  and  $TiO_2$ . (c) UV-Vis diffuse reflectance spectra of  $[Fe^{II}(dcbpy)_3]/TiO_2$ ,  $H_2dcbpy/TiO_2$  and  $TiO_2$ . (d) UV-Vis absorption spectra of  $[Fe^{II}(dcbpy)_3]$  and  $H_2dcbpy$ .)*

*(Embed Table 2. Crystal characteristics of  $[Fe^{II}(dcbpy)_3]/TiO_2$  prepared at different temperatures)*

The Raman spectrum of  $[Fe^{II}(dcbpy)_3]/TiO_2$  (prepared at 100 °C and used in the following



experiments.) is shown in Fig. 2b. Four narrow bands at  $143.11\text{cm}^{-1}$ ,  $397.33\text{cm}^{-1}$ ,  $517.33\text{cm}^{-1}$ , and  $640\text{cm}^{-1}$  can be attributed to the Raman-active modes of  $\text{TiO}_2$  anatase phase with the symmetries of  $E_g$ ,  $B_{1g}$ ,  $A_{1g}$  and  $E_g$ , respectively. From the inset in Fig. 2b, we can identify bands derived from  $[\text{Fe}^{\text{II}}(\text{dcbpy})_3]$  complex. Scattering peak located at  $1618.93\text{cm}^{-1}$  is from the C=O vibration of carboxyl group. Two peaks at  $1550.67\text{cm}^{-1}$  and  $1479.73\text{cm}^{-1}$  belong to the C=C and C=N stretching vibrations of pyridine ring. While peak at  $1266.93\text{cm}^{-1}$  and its shoulder peak  $1295.73\text{cm}^{-1}$  are attributed to  $\delta(\text{C-H})$  ring breathing <sup>[21]</sup>. These Raman scattering peaks confirmed the effective bonding of  $\text{TiO}_2$  and  $[\text{Fe}^{\text{II}}(\text{dcbpy})_3]$  complex.

The UV-vis diffuse reflectance spectrum of  $[\text{Fe}^{\text{II}}(\text{dcbpy})_3]/\text{TiO}_2$  can be seen from figure 2c. Comparing to that of pure  $\text{TiO}_2$  a broad absorption around 550nm in visible light region appeared which results the band gap of this composite changing from 3.2eV to 2.04eV (calculated with Tauc plots). It indicated that the absorption band edge of  $\text{TiO}_2$  obviously extends to the visible light after bonding with  $[\text{Fe}^{\text{II}}(\text{dcbpy})_3]$  complex. In order to confirm the effect of  $[\text{Fe}^{\text{II}}(\text{dcbpy})_3]$  complex on the visible light absorption property of  $\text{TiO}_2$ , the absorption spectra of  $[\text{Fe}^{\text{II}}(\text{dcbpy})_3]$  and  $\text{H}_2\text{dcbpy}$  with same concentration were tested and shown in figure 2d. There are three obvious absorption peaks around 300nm, 380nm and 550nm, respectively, for complex  $[\text{Fe}^{\text{II}}(\text{dcbpy})_3]$ . Comparing to an intense peak appeared around 300nm for  $\text{H}_2\text{dcbpy}$ , which is attributed to ligand-centered (LC)  $\pi \rightarrow \pi^*$  transition band, the coordination effect caused a little blue shift of this  $\pi \rightarrow \pi^*$  transfer for  $[\text{Fe}^{\text{II}}(\text{dcbpy})_3]$ . From Figure 1 we can see complex  $[\text{Fe}^{\text{II}}(\text{dcbpy})_3]$  is in deep pink color which indicated it must absorb visible light from 470nm to 550nm. However, the energy level of  $\pi^*$  of ligand  $\text{H}_2\text{dcbpy}$  is low deriving from its unsaturated structure, so the absorption band centered at 550nm is determined to come from  $d-\pi^*$  metal-to-ligand charge transfer. It is the main

reason that visible light can be used to excited and the band gap of  $[\text{Fe}^{\text{II}}(\text{dcbpy})_3]/\text{TiO}_2$  decreased. Because six 3d electrons of central ion  $\text{Fe}^{2+}$  presence in low spin states and the energy splitting under the action of octahedron ligand field, weak bands from 350 to 400nm and a shoulder peak at 500nm derived from  ${}^1A_{1g} \rightarrow {}^1T_{2g}$  and  ${}^1A_{1g} \rightarrow {}^1T_{1g}$  d-d electron transfer of  $\text{Fe}^{2+}$  ion, respectively.

The SEM and TEM images, and EDS analysis of  $[\text{Fe}^{\text{II}}(\text{dcbpy})_3]/\text{TiO}_2$  are presented in Fig.3. The agglomeration of irregular grains is noticeable in SEM image. The TEM image shows a hexagon structure. The particle size is in range of 20-25nm, which is in good agreement with the XRD analysis. The presence of N, C, Fe elements in the EDS spectrum of  $[\text{Fe}^{\text{II}}(\text{dcbpy})_3]/\text{TiO}_2$  confirms that the  $[\text{Fe}^{\text{II}}(\text{dcbpy})_3]$  complex has successfully bound to the surface of  $\text{TiO}_2$ .

*(Embed Figure 3. (a) SEM image, (b) TEM image, (c) EDS analysis of  $[\text{Fe}^{\text{II}}(\text{dcbpy})_3]/\text{TiO}_2$ )*

XPS results in Fig. 4 provide further evidence that Fe-complexes indeed formed nanocomposites with  $\text{TiO}_2$ . Peaks of Fe  $2p_{1/2}$  and Fe  $2p_{3/2}$  are detected a 711 eV and 723 eV. Peaks at 458.3 eV and 464.1 eV are assigned to Ti  $2p_{3/2}$  and Ti  $2p_{1/2}$ . The distance between these two peaks, 5.8 eV, indicates that the crystal structure of  $\text{TiO}_2$  remains the same after forming composite with  $[\text{Fe}^{\text{II}}(\text{dcbpy})_3]$  complex. The appearance of peaks C  $1s$ , O  $1s$ , and N  $1s$  illustrate the surface of  $\text{TiO}_2$  has been contaminated by organic compounds. Peak at 529.48 eV belonging to lattice oxygen (Ti-O-Ti) in bulk phase of  $\text{TiO}_2$  are detected together with two other peaks at 531.48eV and 532.64eV that arise from hydroxyl oxygen (-OH) and C-O bond on the surface of  $\text{TiO}_2$ . The calculated atomic ratio of N /Fe, 6.6, establishes a 1:3 molar ratio of  $\text{Fe}(\text{II}): \text{H}_2\text{dcbpy}$ .

*(Embed Figure 4. XPS spectra of [Fe<sup>II</sup>(dcbpy)<sub>3</sub>]/TiO<sub>2</sub>)*

### *3.2 Photoactivity and photostability of [Fe<sup>II</sup>(dcbpy)<sub>3</sub>]/TiO<sub>2</sub>*

The results of photocatalytic degradation of phenol by TiO<sub>2</sub>, H<sub>2</sub>dcbpy/TiO<sub>2</sub> and [Fe<sup>II</sup>(dcbpy)<sub>3</sub>]/TiO<sub>2</sub> under visible light and the recycling stability of H<sub>2</sub>dcbpy/TiO<sub>2</sub> and [Fe<sup>II</sup>(dcbpy)<sub>3</sub>]/TiO<sub>2</sub> are presented in Fig. 5. In the absence of photocatalyst, no degradation of phenol is detected by visible light irradiation for as long as 120 min. The same result is obtained with a mixture of phenol and photocatalyst in the absence of visible light irradiation. In the presence of TiO<sub>2</sub>, the degradation of phenol reaches only 14.3% after 80 min irradiation. Using H<sub>2</sub>dcbpy/TiO<sub>2</sub> or [Fe<sup>II</sup>(dcbpy)<sub>3</sub>]/TiO<sub>2</sub> as the photocatalyst, 75.0%, and 95.1% of phenol can be decomposed under the same condition. From 80 to 120 min only a small increase (1.7%) in the degradation of phenol by using [Fe<sup>II</sup>(dcbpy)<sub>3</sub>]/TiO<sub>2</sub> achieved while that of 17.4% increase by using H<sub>2</sub>dcbpy/TiO<sub>2</sub> obtained. It indicated that the degradation efficiency is quite different during 80 min when [Fe<sup>II</sup>(dcbpy)<sub>3</sub>]/TiO<sub>2</sub> and H<sub>2</sub>dcbpy/TiO<sub>2</sub> are employed. The degradation rate of phenol by these three different photocatalysts can be derived from the kinetic curve fitting shown in Fig. 5b. The rate constants (*k*) for using TiO<sub>2</sub>, H<sub>2</sub>dcbpy/TiO<sub>2</sub>, and [Fe<sup>II</sup>(dcbpy)<sub>3</sub>]/TiO<sub>2</sub> as photocatalyst, are 0.00194 min<sup>-1</sup>, 0.01674 min<sup>-1</sup>, and 0.03697 min<sup>-1</sup>, respectively. Because of the effective sensitization [Fe<sup>II</sup>(dcbpy)<sub>3</sub>] complex to TiO<sub>2</sub>, the photocatalytic degradation rate of phenol by using [Fe<sup>II</sup>(dcbpy)<sub>3</sub>]/TiO<sub>2</sub> is about 2.2 times and 18 times higher than those of H<sub>2</sub>dcbpy/TiO<sub>2</sub> and TiO<sub>2</sub>.

*(Embed Figure 5. (a) Photocatalytic degradation of phenol by TiO<sub>2</sub>, H<sub>2</sub>dcbpy/TiO<sub>2</sub> and [Fe<sup>II</sup>(dcbpy)<sub>3</sub>]/TiO<sub>2</sub> under visible light. (b) Kinetic curve fitting of the photocatalytic degradation*

of phenol. (c) Recycling stability of prepared  $[\text{Fe}^{\text{II}}(\text{dcbpy})_3]/\text{TiO}_2$  and  $\text{H}_2\text{dcbpy}/\text{TiO}_2$ . (d) Photoelectrochemistry performance of  $\text{TiO}_2$ ,  $\text{H}_2\text{dcbpy}/\text{TiO}_2$  and  $[\text{Fe}^{\text{II}}(\text{dcbpy})_3]/\text{TiO}_2$

The recycled photocatalytic experiments are carried out to test the stability of the photocatalysts and the results are presented in Fig. 5c. The degradation efficiency of phenol decreases from 96.8% for fresh  $[\text{Fe}^{\text{II}}(\text{dcbpy})_3]/\text{TiO}_2$ , to 86.1% and 77.5% when it was used for the second and the third time. The decrease is more significant for  $\text{H}_2\text{dcbpy}/\text{TiO}_2$ , dropping from 92.4% to 70.1% and 50.3% under the same condition. Although the photocatalytic degradation efficiency of phenol using  $\text{H}_2\text{dcbpy}/\text{TiO}_2$  and  $[\text{Fe}^{\text{II}}(\text{dcbpy})_3]/\text{TiO}_2$  are almost the same (92.4% and 96.8%) after 2h, the photostability of  $[\text{Fe}^{\text{II}}(\text{dcbpy})_3]/\text{TiO}_2$  is higher. The decreasing of degradation efficiency in both cases in the repeated use may be due to the loss of loosely adsorbed  $[\text{Fe}^{\text{II}}(\text{dcbpy})_3]$  complex or  $\text{H}_2\text{dcbpy}$  molecules on the surface of  $\text{TiO}_2$  during the washing process between each recycling test.

To verify the effects of  $[\text{Fe}^{\text{II}}(\text{dcbpy})_3]$  on the interface electron transfer between complex and  $\text{TiO}_2$ , the photocurrent density of  $[\text{Fe}^{\text{II}}(\text{dcbpy})_3]/\text{TiO}_2$  is recorded and given in Fig.5d. It is obvious that the photocurrent densities derived from  $\text{TiO}_2$ ,  $\text{H}_2\text{dcbpy}/\text{TiO}_2$  and  $[\text{Fe}^{\text{II}}(\text{dcbpy})_3]/\text{TiO}_2$  are quite different when they are under visible light irradiation. As soon as the visible light was turned on, the photocurrent densities for both  $\text{H}_2\text{dcbpy}/\text{TiO}_2$  and  $[\text{Fe}^{\text{II}}(\text{dcbpy})_3]/\text{TiO}_2$  reached their highest value, with faster response to visible light than  $\text{TiO}_2$ . During the process of irradiation the photocurrent densities of all three catalysts changed slightly after ten circles, showing good photostability. The photocurrent densities increase as this follow:  $\text{TiO}_2 < \text{H}_2\text{dcbpy}/\text{TiO}_2 < [\text{Fe}^{\text{II}}(\text{dcbpy})_3]/\text{TiO}_2$ . The higher the photocurrent density means the longer the lifetime of photo-generated charges, thus the better photocatalytic activity. It is no surprise that the best photocatalytic activity is found for

$[\text{Fe}^{\text{II}}(\text{dcbpy})_3]/\text{TiO}_2$ , which is coincident with the experimental results of photocatalytic degradation of phenol by  $\text{TiO}_2$ ,  $\text{H}_2\text{dcbpy}/\text{TiO}_2$  and  $[\text{Fe}^{\text{II}}(\text{dcbpy})_3]/\text{TiO}_2$  under visible light above.

Here there are two issues that need to be discussed. First, why the photocatalytic reaction rate of  $[\text{Fe}^{\text{II}}(\text{dcbpy})_3]/\text{TiO}_2$  is faster than that of  $\text{H}_2\text{dcbpy}/\text{TiO}_2$ ? Second, why the photostability of  $\text{H}_2\text{dcbpy}/\text{TiO}_2$  is obviously weaker than that of  $[\text{Fe}^{\text{II}}(\text{dcbpy})_3]/\text{TiO}_2$  during the recycling process?

As we know the visible light absorption and interfacial electron transfer are two crucial factors determining the photocatalytic activity and photocatalytic reaction rate<sup>[15]</sup>. Firstly, from Fig. 2c we have known that a more effective performance to absorb visible light in  $[\text{Fe}^{\text{II}}(\text{dcbpy})_3]/\text{TiO}_2$  can be reflected by the appearance of absorption band around 550nm derived from M-L charge transfer of complex. However, in  $\text{H}_2\text{dcbpy}/\text{TiO}_2$  the intrinsic absorption of  $\text{TiO}_2$  did not change a lot but the absorption band edge extended to about 500nm. It indicated that  $\text{H}_2\text{dcbpy}$  had some effects on the visible light absorption of  $\text{TiO}_2$  but it is not very significant. So the visible light harvesting of  $\text{H}_2\text{dcbpy}/\text{TiO}_2$  is obviously weakened than that of  $[\text{Fe}^{\text{II}}(\text{dcbpy})_3]/\text{TiO}_2$ . Secondly, there are six free carboxyl groups in  $[\text{Fe}^{\text{II}}(\text{dcbpy})_3]$  complex which can connect less than or equal to six  $\text{TiO}_2$  molecules simultaneously (see Fig.6a and 6b), so that there are more directions or pathways in this like a network structure centered by  $[\text{Fe}^{\text{II}}(\text{dcbpy})_3]$  complex can be applied to the electron transfer from metal to ligand and to conduction band of  $\text{TiO}_2$  further synchronously. And the free rotation of  $\sigma$  bonds between two pyridine rings were limited due to the formation of chelate compound  $[\text{Fe}^{\text{II}}(\text{dcbpy})_3]$  and so caused the increase of conjugate plane. The attachment of  $[\text{Fe}^{\text{II}}(\text{dcbpy})_3]$  complex on the surface of  $\text{TiO}_2$  via its one or two anchoring carboxyl groups provide a more compact and ordered arrangement which is obviously beneficial to the electron injection. In contrast, only two electron transfer accesses (see Fig.6c and 6d) from

ligand to  $\text{TiO}_2$  can be used in  $\text{H}_2\text{dcbpy}/\text{TiO}_2$ . Meanwhile, it is very difficult to generate a stable conjugate plane because of the free rotation of  $\sigma$  bond between two pyridine rings. From Fig. 6c and 6d we can also find there are two possible modes linking  $\text{H}_2\text{dcbpy}$  onto  $\text{TiO}_2$  surface. One is chelating mode via two N atoms of  $\text{H}_2\text{dcbpy}$  coordinating to Ti atom of  $\text{TiO}_2$  surface, and another is the binding of one carboxyl group of  $\text{H}_2\text{dcbpy}$  with Ti of  $\text{TiO}_2$  surface. These two modes compete with each other, causing the disorganization of  $\text{H}_2\text{dcbpy}$  molecules on the surface of  $\text{TiO}_2$ , which may result in poor electron injection to the  $\text{TiO}_2$  conduction band. So that the interfacial electron transfer efficiency in  $\text{H}_2\text{dcbpy}/\text{TiO}_2$  is less than that in  $[\text{Fe}^{\text{II}}(\text{dcbpy})_3]/\text{TiO}_2$ .

At the same time like a network structure with complex  $[\text{Fe}^{\text{II}}(\text{dcbpy})_3]$  as center increased the stability of  $[\text{Fe}^{\text{II}}(\text{dcbpy})_3]/\text{TiO}_2$ . On the one side larger steric hindrance and electrostatic repulsion between  $[\text{Fe}^{\text{II}}(\text{dcbpy})_3]$  complex stop them from each other. On the other side six carboxyl groups are chemically equivalent to bond with  $\text{TiO}_2$ . This complex surrounded by  $\text{TiO}_2$  cannot be attacked by other materials in the photocatalytic suspension system and so caused a better photostability. In contrast, the competition from each other of different chelating modes between  $\text{H}_2\text{dcbpy}$  with  $\text{TiO}_2$  may lead to photocatalysts  $\text{H}_2\text{dcbpy}/\text{TiO}_2$  with different structure coexistence in one photocatalytic suspension system. They may pile up or intertwine together and cause the decrease of photostability.

*(Embed Figure 6. Schematic diagram of linking  $\text{H}_2\text{dcbpy}$  or  $[\text{Fe}^{\text{II}}(\text{dcbpy})_3]$  onto  $\text{TiO}_2$  surface.)*

3.3 Photoactivity and photostability comparison of  $[\text{Fe-dcbpy}]_{\text{complex}}/\text{TiO}_2$ ,  $[\text{Fe-dcbpy-bpy}]_{\text{complex}}/\text{TiO}_2$ , and  $[\text{Fe-dcbpy-phen}]_{\text{complex}}/\text{TiO}_2$

Choi's group [13, 22] have reported the photoactivities of three Ru-complexes,  $[\text{Ru}^{\text{II}}(\text{dcbpy})_3]/\text{TiO}_2$ ,  $[\text{Ru}^{\text{II}}(\text{dcbpy})_2(\text{bpy})]/\text{TiO}_2$  and  $[\text{Ru}^{\text{II}}(\text{dcbpy})(\text{bpy})_2]/\text{TiO}_2$  via DSSC and production of hydrogen. They found that the surface binding on  $\text{TiO}_2$  and the overall cell performance were highly dependent on the number of anchoring groups. As a result,  $[\text{Ru}^{\text{II}}(\text{dcbpy})_2(\text{bpy})]/\text{TiO}_2$  showed the best cell performance despite the lowest visible light absorption because the most effective surface binding mode is allowed with this structure. However,  $[\text{Ru}^{\text{II}}(\text{dcbpy})_3]/\text{TiO}_2$  showed the highest hydrogen production because of the highest surface absorption concentration in the presence of EDTA and the highest molar absorptivity in the visible region. They thought that the absorption of these Ru complexes on  $\text{TiO}_2$  in the presence of EDTA should be weak physical attraction, and their sensitizing capability is strongly limited, regardless of number of carboxylate groups. In order to reveal the mechanism of Fe complex sensitized  $\text{TiO}_2$  during the photocatalytic degradation of phenol, the photoactivities of  $[\text{Fe}^{\text{II}}(\text{dcbpy})_2(\text{bpy})]/\text{TiO}_2$  and  $[\text{Fe}^{\text{II}}(\text{dcbpy})(\text{bpy})_2]/\text{TiO}_2$  together with  $[\text{Fe}^{\text{II}}(\text{dcbpy})_2(\text{phen})]/\text{TiO}_2$  and  $[\text{Fe}^{\text{II}}(\text{dcbpy})(\text{phen})_2]/\text{TiO}_2$ , are investigated, and the results are presented in Fig.7.

From Fig. 7a we obtain the rate constants ( $k$ ) for  $[\text{Fe}^{\text{II}}(\text{dcbpy})_3]/\text{TiO}_2$ ,  $[\text{Fe}^{\text{II}}(\text{dcbpy})_2(\text{bpy})]/\text{TiO}_2$ ,  $[\text{Fe}^{\text{II}}(\text{dcbpy})(\text{bpy})_2]/\text{TiO}_2$ ,  $[\text{Fe}^{\text{II}}(\text{dcbpy})_2(\text{phen})]/\text{TiO}_2$ , and  $[\text{Fe}^{\text{II}}(\text{dcbpy})(\text{phen})_2]/\text{TiO}_2$ , which are 0.0355, 0.0270, 0.0260, 0.0299, and 0.0439, respectively. The photocatalytic activities of the five photocatalysts can be arranged as  $[\text{Fe}^{\text{II}}(\text{dcbpy})(\text{bpy})_2]/\text{TiO}_2 < [\text{Fe}^{\text{II}}(\text{dcbpy})_2(\text{bpy})]/\text{TiO}_2 < [\text{Fe}^{\text{II}}(\text{dcbpy})_2(\text{phen})]/\text{TiO}_2 < [\text{Fe}^{\text{II}}(\text{dcbpy})_3]/\text{TiO}_2 < [\text{Fe}^{\text{II}}(\text{dcbpy})(\text{phen})_2]/\text{TiO}_2$ . It is obvious that the photocatalytic activities of these materials are related to not only the number of anchoring groups but also the conjugated structure of Fe complexes. Increasing the number of anchoring group  $-\text{COOH}$  and extending the conjugate plane

of complexes cause the increase of photocatalytic activity of photocatalyst. It is worth noting that the photocatalytic degradation efficiency of phenol by  $[\text{Fe}^{\text{II}}(\text{dcbpy})(\text{phen})_2]/\text{TiO}_2$  is the highest among these five materials even its number of anchoring group is only two, suggesting that the effect of conjugate structure on the photocatalytic activity under visible light is stronger than that of number of anchoring group.

*(Embed Figure 7. (a) Kinetic curve fitting of the photocatalytic degradation of phenol. (b) Recycling stability. (c) UV-Vis absorption and diffuse reflectance spectra. (d) Photoelectrochemistry performance of five Fe complex/TiO<sub>2</sub> compounds.)*

Similarly, conjugate plane sizes and anchoring group numbers of Fe complexes are closely related to the photochemical stability. In the five photocatalysts  $[\text{Fe}^{\text{II}}(\text{dcbpy})(\text{phen})_2]/\text{TiO}_2$  shows the best stability (see Fig. 7b). 99.3%, 93.7% and 90.2% of phenol is decomposed after the first, second and third usage of  $[\text{Fe}^{\text{II}}(\text{dcbpy})(\text{phen})_2]/\text{TiO}_2$ . The stability of  $[\text{Fe}^{\text{II}}(\text{dcbpy})_3]/\text{TiO}_2$  is less than  $[\text{Fe}^{\text{II}}(\text{dcbpy})(\text{phen})_2]/\text{TiO}_2$ , the photocatalytic degradation efficiency of phenol decreases from 96.8% to 77.5% when  $[\text{Fe}^{\text{II}}(\text{dcbpy})_3]/\text{TiO}_2$  is repeatedly used the third time. It is clear that the recycling stabilities of these five photocatalysts decreased greatly when anchoring group ( $-\text{COOH}$ ) number and conjugate plane of Fe complexes reduced. By contrast, the recycling stability of  $[\text{Fe}^{\text{II}}(\text{dcbpy})_2(\text{phen})]/\text{TiO}_2$  does not decline very much, which demonstrated the conjugate structure of phenanthroline plays an important role on the photocatalyst's stability.

Visible light absorption property is one of the critical factors that determine the photocatalytic performance of Fe complex/ $\text{TiO}_2$ . Comparing the UV-vis diffuse reflectance spectra of these photocatalysts (shown in Fig. 7c) we can see that the intrinsic absorption of  $\text{TiO}_2$



have not been changed after bonding with Fe complex, but there are small difference appeared around 550nm, which derived from d- $\pi^*$  metal-to-ligand charge transfer in different Fe complex. The absorption peak of  $[\text{Fe}^{\text{II}}(\text{dcbpy})(\text{phen})_2]/\text{TiO}_2$  appears at 551.6nm, which red shifts of  $[\text{Fe}^{\text{II}}(\text{dcbpy})_3]/\text{TiO}_2$  than 8.4nm. The absorption band edge in visible light of  $[\text{Fe}^{\text{II}}(\text{dcbpy})(\text{phen})_2]/\text{TiO}_2$ ,  $[\text{Fe}^{\text{II}}(\text{dcbpy})_3]/\text{TiO}_2$  and  $[\text{Fe}^{\text{II}}(\text{dcbpy})_2(\text{phen})]/\text{TiO}_2$  are more broader than that of  $[\text{Fe}^{\text{II}}(\text{dcbpy})(\text{bpy})_2]/\text{TiO}_2$  and  $[\text{Fe}^{\text{II}}(\text{dcbpy})_2(\text{bpy})]/\text{TiO}_2$ . The band gaps of these five composites are calculated by using Tauc plots. They are 2.08eV, 2.05eV, 2.09eV, 2.10eV and 2.09eV for  $[\text{Fe}^{\text{II}}(\text{dcbpy})_3]/\text{TiO}_2$ ,  $[\text{Fe}^{\text{II}}(\text{dcbpy})(\text{phen})_2]/\text{TiO}_2$ ,  $[\text{Fe}^{\text{II}}(\text{dcbpy})_2(\text{phen})]/\text{TiO}_2$ ,  $[\text{Fe}^{\text{II}}(\text{dcbpy})(\text{bpy})_2]/\text{TiO}_2$  and  $[\text{Fe}^{\text{II}}(\text{dcbpy})_2(\text{bpy})]/\text{TiO}_2$ . Thus it can be seen that the visible light absorption of  $[\text{Fe}^{\text{II}}(\text{dcbpy})(\text{phen})_2]/\text{TiO}_2$  is stronger than that of other four materials. It is one of main reasons causing its enhanced photocatalytic activity.

Interface electron transfer between Fe complex and surface of  $\text{TiO}_2$  is another key factor that deciding the photocatalytic activity of Fe complex/ $\text{TiO}_2$ . The test results of photoelectrochemistry performance of five Fe complex/ $\text{TiO}_2$  compounds are shown in Fig. 7d. As the visible light was turned on, the photocurrent densities for these five materials reached their highest value, 12.04、11.52、9.94、8.80、6.57  $\mu\text{A}/\text{cm}^2$  for  $[\text{Fe}^{\text{II}}(\text{dcbpy})(\text{phen})_2]/\text{TiO}_2$ ,  $[\text{Fe}^{\text{II}}(\text{dcbpy})_3]/\text{TiO}_2$ ,  $[\text{Fe}^{\text{II}}(\text{dcbpy})_2(\text{phen})]/\text{TiO}_2$ ,  $[\text{Fe}^{\text{II}}(\text{dcbpy})_2(\text{bpy})]/\text{TiO}_2$  and  $[\text{Fe}^{\text{II}}(\text{dcbpy})(\text{bpy})_2]/\text{TiO}_2$ . During the irradiation process their photocurrent densities decreased slowly after ten circles, showing good photostability. The photocurrent densities of  $[\text{Fe}^{\text{II}}(\text{dcbpy})(\text{phen})_2]/\text{TiO}_2$  and  $[\text{Fe}^{\text{II}}(\text{dcbpy})_3]/\text{TiO}_2$  are nearly identical, which higher than that of other three photocatalysts. The higher the photocurrent density means the faster electron transfer and the longer lifetime of photo-generated charges, thus the better photocatalytic activity. It is no surprise that the increase of conjugate plane derived from

phenanthroline instead of H<sub>2</sub>dc bpy caused the enhanced performance of interface electron transfer.

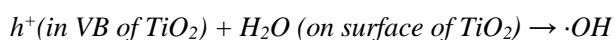
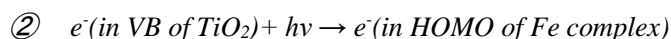
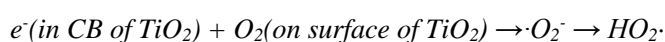
In order to gain insight into the mechanism of interface electron transfer of Fe complex/TiO<sub>2</sub> photocatalysts, the cyclic voltammetry of five different catalysts is performed and the results are shown in Table 3. The energies of HOMO and LOMO are calculated according to the following formulas:

$$\text{HOMO} = -4.72 - E(\text{ox})$$

$$\text{LOMO} = \text{HOMO} + E_g$$

*(Embed Table 3. Oxidation potentials of Fe complex and calculated HOMO and LOMO energy levels)*

On the basis of the above calculation, the mechanism of electron transfer process between Fe complexes and TiO<sub>2</sub> is illustrated in Fig. 9 and described in detail as follows:



*(Embed Figure 8. Schematic illustration of energy level of Fe complex and TiO<sub>2</sub> and probable electron transfer process)*

It also can be found that the energy level of HOMO and LUMO of [Fe<sup>II</sup>(dc bpy)(phen)<sub>2</sub>] and [Fe<sup>II</sup>(dc bpy)<sub>2</sub>(phen)] are increased as compared to that of [Fe<sup>II</sup>(dc bpy)<sub>3</sub>]. There is almost no difference on the energy level of HOMO and LUMO when one or two dc bpy ligands are replaced

by bpy ligands. Furthermore, with the introduction of phen ligands the distance between HOMO of complex and conduction band of TiO<sub>2</sub> decreased. So, the electrons on the HOMO of [Fe<sup>II</sup>(dcbpy)(phen)<sub>2</sub>] and [Fe<sup>II</sup>(dcbpy)<sub>2</sub>(phen)] are prefer to injected to the conduction band of TiO<sub>2</sub> directly when they obtained visible light irradiation, because the energy difference between HOMO of complex and CB of TiO<sub>2</sub> is less than the difference between HOMO and LUMO of complex. Obviously, the linkage of carboxyl group of Fe complex with TiO<sub>2</sub> created conditions for this migration. The smaller the difference between HOMO of complex and CB of TiO<sub>2</sub>, the easier electron migration, and so caused the faster photocatalytic reaction if the electrons subsequently captured by the oxygen adsorbed on the surface of TiO<sub>2</sub> to generate a series of active oxygen species. It is probably the main reason that the photocatalytic performance of [Fe<sup>II</sup>(dcbpy)(phen)<sub>2</sub>]/TiO<sub>2</sub> is stronger than that of [Fe<sup>II</sup>(dcbpy)<sub>3</sub>]/TiO<sub>2</sub>. At the same time, under the visible irradiation electrons on the VB of TiO<sub>2</sub> can transfer to the HOMO of Fe complex. On the one hand, it can supply sufficient electrons for HOMO to enable the photocatalytic reaction to continue, via electrons transfer from HOMO to CB of TiO<sub>2</sub> subsequently. On the other hand, holes thus produced can reacted with water on the surface of TiO<sub>2</sub> and generated hydroxyl radicals to participate in the oxidation reduction reaction of phenol. Nevertheless, we have also noticed that the photocatalytic degradation efficiency of phenol by [Fe<sup>II</sup>(dcbpy)<sub>2</sub>(phen)]/TiO<sub>2</sub> is less than that of that of [Fe<sup>II</sup>(dcbpy)<sub>3</sub>]/TiO<sub>2</sub> though the difference between HOMO of [Fe<sup>II</sup>(dcbpy)<sub>2</sub>(phen)] and CB of TiO<sub>2</sub> is less than that of [Fe<sup>II</sup>(dcbpy)<sub>3</sub>]. So, besides the influence of conjugate structure derived from phen, the number of carboxyl group and thus produced more electron transfer pathways may be another key reason to obtain enhanced photocatalytic activity. Their cooperation plays important roles on improving photocatalytic performance of photocatalyst.

#### 4 Conclusions

The visible light photocatalytic activity of TiO<sub>2</sub> can be enhanced greatly by combining with these five Fe complexes, [Fe<sup>II</sup>(dcbpy)<sub>3</sub>], [Fe<sup>II</sup>(dcbpy)(phen)<sub>2</sub>], [Fe<sup>II</sup>(dcbpy)<sub>2</sub>(phen)], [Fe<sup>II</sup>(dcbpy)<sub>2</sub>(bpy)] and [Fe<sup>II</sup>(dcbpy)(bpy)<sub>2</sub>]. The highest photocatalytic degradation efficiency of phenol is achieved when [Fe<sup>II</sup>(dcbpy)(phen)<sub>2</sub>]/TiO<sub>2</sub> is applied to the photocatalytic system. About 99.3% of phenol was photodegraded under visible light irradiation during 2h. It also exhibited an excellent photostability after third recycling. It is found that the interfacial interaction between Fe complex and TiO<sub>2</sub> is closely related to the anchoring group number and conjugated structure of Fe complex. Because more anchoring groups may supply more electron transfer pathways from complex to TiO<sub>2</sub> and bigger conjugated structure may accelerate the electron transfer and photoelectric response efficiency. Both of them are beneficial to improve the photocatalytic performance of TiO<sub>2</sub>. According to our test results electrons on HOMO of Fe complex may transfer to the CB of TiO<sub>2</sub> directly under visible light irradiation. It provides a chance for electrons on VB of TiO<sub>2</sub> to transfer to this HOMO of Fe complex then. So, both of electrons and holes can be captured by O<sub>2</sub> and H<sub>2</sub>O on the surface of TiO<sub>2</sub> to generate a series of active oxygen species, which dominate the decomposition of phenol.

#### Acknowledgements

The authors would like to acknowledge the financial support by National Natural Science Foundation of China NSFC (21573039, 51102042), Jilin Province Science and Technology Development Project (20140414021GH, 200905932), Jilin Province Environmental Protection Department Project (2008-22), and Jilin Province Personnel Department Project for supporting

study abroad and return.

## References

- [1] G. Granados O., C.-A. Páez M., F. Martínez O., E.-A. Páez-Mozo, *Catal. Today* 107-108 (2005) 589-594.
- [2] G. Xiao, X. Huang, X.-P. Liao, B. Shi, *J. Phys. Chem. C* 117 (2013) 9739–9746.
- [3] B. Sambandam, A. Surenjan, L. Philip, T. Pradeep, *ACS Sustainable Chem. Eng.* 3 (2015) 1321-1329.
- [4] X.-C. Li, G.-L. Jiang, G.-H. He, W.-J. Zheng, Y. Tan, W. Xiao, *Chemical Engineering Journal* 236 (2014) 480–489.
- [5] T. Sreethawong, C. Junbua, S. Chavadej, *J. Power Sources* 190 (2009) 513–524.
- [6] Y. Park, S.-H. Lee, S.-O. Kang, W. Choi, *Chem. Commun.* 46 (2010) 2477-2479.
- [7] M.-Q. Wang, X.-G. Wang, *Solar Energy Materials and Solar Cells* 91 (2007) 1782-1787.
- [8] X.-Z. Zheng, D.-Z. Li, X.-F. Li, J. Chen, C.-S. Cao, J.-L. Fang, J.-B. Wang, Y.-H. He, Y. Zheng, *Appl. Catal. B* 168-169 (2015) 408–415.
- [9] G.-J. Ai, R. Mo, H. Xu, Q. Chen, S. Yang, H.-X. Li, J.-X. Zhong, *J. Power Sources* 280 (2015) 5–11.
- [10] S. Afzal, W.-A. Daoud, S.-J. Langford, *ACS Appl. Mater. Interfaces* 5 (2013) 4753-4759.
- [11] U. Veikko, X.-H. Zhang, T.-Y. Peng, P. Cai, G.-Z. Cheng, *Spectrochimica Acta Part A: Molecular and Biomolecular Spectroscopy* 105 (2013) 539–544.
- [12] W.-J. Song, A. Ito, R.-A. Binstead, K. Hanson, H.-L. Luo, M.-K. Brennaman, J.-J. Concepcion, T.-J. Meyer, *J. Am. Chem. Soc.* 135 (2013) 11587–11594.
- [13] E. Bae, W. Choi, *J. Phys. Chem. B* 110 (2006) 14792–14799.
- [14] X. Chen, W.-H. Ma, J. Li, Z.-H. Wang, C.-C. Chen, H.-W. Ji, J.-C. Zhao, *J. Phys. Chem. C* 115 (2011) 4089–4095.
- [15] V. Thavasi, V. Renugopalakrishnan, R. Jose, S. Ramakrishna, *Mater. Sci. Eng. R* 63 (2009) 81–99.
- [16] Y. Cho, W. Choi, C.-H. Lee, T. Hyeon, H.-L. Lee, *Environ. Sci. Technol.* 35 (2011) 966–970.
- [17] E. Bae, W. Choi, *Environ. Sci. Technol.* 37 (2003) 147–152.
- [18] E. Bae, W. Choi, J. Park, H.-S. Shin, S.-B. Kim, J.-S. Lee, *J. Phys. Chem. B* 108 (2004) 14093–14101.
- [19] R. Dagherir, P. Drogui, D. Robert, *Ind. Eng. Chem. Res.* 52 (2013) 3581–3599.
- [20] Y.-W. Huang, Q.-K. Shang, D. Wang, S. Yang, H.-Y. Guan, Q. Lu, S.-C. Tsang, *Appl. Catal. B* 187 (2016) 59–66.
- [21] X.-M. Shi, H.-Y. Wang, Y.-B. Li, J.-X. Yang, L. Chen, G. Hui, W.-Q. Xu, B. Zhao, *Chemical Research in Chinese Universities* 26 (2010) 1011-1015.
- [22] H. Park, E. Bae, J.-J. Lee, J. Park, W. Choi, *J. Phys. Chem. B* 110 (2006) 8740-8749.